Journal of Energy Storage 72 (2023) 108234

Contents lists available at ScienceDirect

Journal of Energy Storage

journal homepage: www.elsevier.com/locate/est

Research papers

Electrochemical polarization-based fast charging of lithium-ion batteries in embedded systems

C. Zoerr [a,b,*], J.J. Sturm [a], S. Solchenbach [a], S.V. Erhard [a], A. Latz [b]

[a] BMW Group, 80788 Munich, Germany
[b] Helmholtz Institute Ulm for Electrochemical Energy Storage, 89081 Ulm, Germany

ARTICLE INFO

Keywords:
Fast charging
P2D model
Lithium plating
Anode potential
Polarization

ABSTRACT

The deposition of metallic lithium on the negative electrode's surface of a lithium-ion battery, known as lithium plating, can significantly reduce the battery's cycle life, performance, and safety. The likelihood of the lithium plating reaction depends on the current rate, temperature, and the state of charge (SOC), which complicates the prediction of this phenomenon. In this paper, a novel fast charging procedure is introduced. It utilizes a correlation between the negative electrode's polarization and the anode potential for current regulation. The correlation is investigated under various operational parameters. Thereby, a linear relation between cell voltage and anode potential is shown independently of the current rate, temperature, and the initial SOC. Based on the linear relation, an anode potential regulation is implemented. In this regard, a Newman-type P2D modeling framework is used to derive a dynamic voltage threshold. Due to the anode potential regulation, the risk of unwanted lithium plating is significantly reduced. The implementation is considered not to require a P2D model on a micro-controller, which is a significant advantage, especially in embedded systems.

1. Introduction

Range anxiety and long charging times are the main factors hindering the large-scale deployment of Battery Electric Vehicles (BEVs) [1–5]. As a result, the field of lithium-ion battery fast charging has gained significant attention [2]. Thereby, electrode active materials with small particle sizes and different battery designs with reduced electrode loadings [2,5] are being studied. Additionally, efforts are made to optimize thermal management [5,6] and to develop new fast charging procedures [1,2,5,7]. However, it has been shown that simply increasing the current rate in a constant-current (CC) constant-voltage (CV) charging procedure accelerates battery degradation. This is primarily attributed to the deposition of metallic lithium on the negative electrode's surface, a phenomenon known as lithium plating [7–11]. The lithium plating reaction is thermodynamically likely if the anode potential falls below 0 V vs. Li/Li^+ at the interface between the negative electrode and the separator [12–14]. However, conventional fast charging protocols, such as CCCV or multi-stage CC protocols, typically utilize predefined current and/or voltage limits. The physical phenomena occurring within the battery cell during the fast charging process are typically ignored [2,15]. The fast charging procedure introduced by Sieg [13] for instance uses current profiles stored in a 2D look-up table as a function of the battery's SOC and its temperature. The applicable charging current, which avoids lithium plating, is determined through measurements using pouch-format three-electrode battery cells. Using the outlined approach, the charging time is reduced without accelerating battery degradation due to lithium plating. The algorithm proposed by Mai [12] applies a predefined voltage ramp to control the charging process. The procedure likewise aims for a reduced charging time without increasing the risk of lithium plating. The voltage ramp is derived from simulating a fast charging procedure using a physics-based battery model. Machine learning based methods that aim for predicting the anode potential in fast charge applications are introduced by Hamar [16] and Lin [17]. Such approaches are often realized as black-box models, not incorporating a profound understanding of the relevant electrochemical processes. More sophisticated approaches employ reduced order physics-based battery models in order to monitor and control the fast charging procedure [2,18,19]. However, these approaches are associated with drawbacks regarding the Random Access Memory (RAM) available on a micro-controller and real-time computability at low processor frequencies [2,19]. Moreover, using physics-based battery models requires an accurate model parameterization under all possible ageing conditions, which is considered a significant constraint of such approaches [20–23].

In this work, we introduce a novel fast charging procedure that incorporates an anode potential regulation to minimize the potential risk of unwanted lithium plating. The anode potential regulation is

* Corresponding author at: BMW Group, 80788 Munich, Germany.
E-mail address: christoph.zoerr@bmw.de (C. Zoerr).

https://doi.org/10.1016/j.est.2023.108234
Received 24 February 2023; Received in revised form 11 June 2023; Accepted 28 June 2023
Available online 12 July 2023

implemented by utilizing a correlation between the negative electrode's polarization and the onset of lithium plating. The correlation was first introduced by Liu [24] using laboratory-format symmetrical cells. The implemented anode potential regulation is considered to provide significant advantages compared to state-of-the-art fast charging algorithms. The novelty of this work comprises: (i) the demonstration of the correlation between the negative electrode's polarization and the lithium plating reaction (indicated by means of the minimum anode potential) in a technologically relevant battery format, (ii) the investigation of the correlation under various current and temperature boundary conditions, and (iii) the derivation of a fast charging procedure that uses the correlation between the negative electrode's polarization and the lithium plating onset for current/voltage control. However, it is to be noted that the experimental validation of the electrochemical-thermal model and the proposed fast charging procedure is part of our ongoing work. This publication hence focuses on the question whether the correlation between the polarization of the negative electrode and the onset current for lithium plating, that is shown in the work of Liu [24] is transferable to a technologically relevant battery format. The correlation is therefore translated into a relation between the anode potential, which is considered an indicator for the lithium plating reaction, and the full cell voltage. In addition, it is analyzed whether the derived relation is suitable for controlling the fast charge procedure in practical applications. Thereby, the influence of electrode-heterogeneities on the accuracy of the implemented anode potential control is discussed. The accuracy with which the novel fast charging procedure controls the anode potential, is subsequently evaluated under varying current and temperature boundary conditions.

The remainder of this work is structured as follows: Section 2 provides an outline of the electrochemical-thermal model used in this study, along with the theoretical considerations that were made beforehand. Additionally, Section 2 describes the simulations conducted to analyze the correlation between the anode potential and the full cell voltage in a technologically relevant battery format. In Section 3, the results of the correlation analysis are presented and discussed, and a novel fast charging procedure is introduced. Subsequently, the introduced procedure is compared to the existing literature in multiple use cases with varying boundary conditions. Section 4 draws a conclusion from the previously discussed simulation results.

2. Method

2.1. Modeling framework

Electrochemical model.— In this work, we employ the widely accepted and extensively discussed Newman-type pseudo-two-dimensional (P2D) model. The objective is to investigate whether a correlation can be identified between the polarization of the battery's negative electrode and the onset of lithium plating, utilizing this model. In this section, we present the model equations that are crucial for a comprehensive understanding of this study. However, for more detailed information on the model, it is referred to the literature [25–27]. Dependent variables of the P2D model are the lithium-ion concentration in the solid active material composite c_s, the lithium-ion concentration in the liquid electrolyte c_l, as well as the potentials of the respective phases Φ_s, and Φ_l. Regarding the lithium-ion concentration in the solid phase, a distinction is made between the surface concentration $c_{s,s}$ and the average concentration $c_{s,\mathrm{ave}}$ of the active material particles. It is solved for these variables along the x-coordinate that represents the thickness of a single electrode stack on a macroscopic scale with two porous electrodes and an electrically insulating separator. The positive and negative electrodes are treated as a volumetric superposition of the solid active material composite and the liquid electrolyte. Lithium-ion diffusion within the solid phase is modeled using a pseudo-dimension (r-coordinate) that represents the radius of an active material particle in the composite of the porous electrode, approximated as symmetric sphere. Since our work does not focus on local mechanisms which might be affected by a particle size distribution, the simplification of symmetrical spheres with an average radius r_P for the active material in the porous electrode is assumed to be reasonable [28]. The two dimensions are coupled via a mass balance and the electrode kinetics. The pore-wall flux of lithium ions at the electrode–electrolyte interface j_n is thereby related to the surface overpotential η according to the Butler–Volmer kinetics

$$\mathrm{F}j_n = i_0 \left(\exp\left(\frac{\alpha_a \mathrm{F}\eta}{\mathrm{R}T} \right) - \exp\left(-\frac{\alpha_c \mathrm{F}\eta}{\mathrm{R}T} \right) \right) \tag{1}$$

with the exchange current density i_0 given by

$$i_0 = \mathrm{F} k_c^{\alpha_a} k_a^{\alpha_c} \left(c_{s,\max} - c_s \right)^{\alpha_a} c_s^{\alpha_c} \left(\frac{c_l}{c_{l,\mathrm{ref}}} \right)^{\alpha_a} \tag{2}$$

where $c_{l,\mathrm{ref}}$ is the reference lithium-ion concentration in the electrolyte, and k_a and k_c are the reaction rate constants for the negative and positive electrode, respectively. The charge transfer coefficients α_a and α_c weight the anodic and cathodic reaction, thereby accounting for the symmetry of the reaction [28]. The surface overpotential η is considered to be the driving force for the electrochemical reaction. It corresponds to the difference between the electrochemical potentials of the surface of an active material particle and the liquid electrolyte in contact with the respective particle

$$\eta(x,t) = \Phi_s(x,t) - \Phi_l(x,t) - E_\mathrm{eq}\left(c_{s,s}(x,t) \right) \tag{3}$$

where Φ_s is the electrical potential of the solid active material composite, Φ_l is the electrochemical potential in the liquid electrolyte and E_eq is the electrode's equilibrium surface potential, which is a function of the surface concentration of the active material particles. The electrical potential of the porous electrode directly contributes to the full cell voltage, which is given by

$$V_\mathrm{cell} = \Phi_s(x,t)\,|_{x=L} - \Phi_s(x,t)\,|_{x=0} - R_\Omega I + \mathrm{const.} \tag{4}$$

where $\Phi_s(x,t)\,|_{x=L}$ and $\Phi_s(x,t)\,|_{x=0}$ are the potentials at the current collecting foils of the positive and negative electrode. The ohmic resistances of the battery's passive components (e.g. the contact resistance at the terminals) are represented by R_Ω. The charge/discharge current is given by I. The subscript L specifies the thickness of the electrode stack. The constant value given in Eq. (4) relates to the difference of the Fermi levels of the positive and negative electrode. The anode potential, considered an indicator for the lithium plating reaction in this study, is defined as the potential drop between the electrical potential of the porous active material composite of the electrode and the potential of the liquid electrolyte ($\Phi_s - \Phi_l$) at the anode-separator interface [12,29]. In this regard, the lithium plating phenomenon is thermodynamically likely if the so-called anode potential $\Phi_\mathrm{An,min}$ falls below 0 V vs. Li/Li$^+$ at this respective point [12–14]. Hence, the condition

$$\Phi_{\mathrm{An,min}=\Phi_s(x,t)|_{x=L_\mathrm{neg}}} - \Phi_l(x,t)\,|_{x=L_\mathrm{neg}} \leq 0 \text{ V vs. Li/Li}^+ \tag{5}$$

represents the onset condition for lithium plating. This simplification is assumed reasonable for our work, as lithium plating is usually initiated at the anode-separator interface according to the literature [9,11,30]. Since the proposed fast charging procedure aims to prevent unwanted lithium plating, it is considered sufficient to consider the minimum anode potential occurring at the anode-separator interface when evaluating the risk of lithium plating. An explicit ageing model incorporating the lithium plating reaction is accordingly not implemented in the modeling framework we used. The parameter set for the electrochemical model used in this work is summarized in Table A.1.

Thermal model.— The electrochemical P2D model is coupled with a zero-dimensional thermal model to account for the temperature dependency of the electrochemical reactions. Thereby, heat generation within the electrode's active material composite and heat exchange with the surroundings is taken into account. However, the local temperature distribution within the cell as well as the heat generation in its passive

electric components (e.g. current collecting foils, and the cells electrical contacts) are neglected in the zero-dimensional model approach. Heat exchange with the surroundings is considered to be dominated by convection. Thus, a simplified energy mass balance that is derived from the work of Bernardi [31] is applied. It is given by

$$\rho V C_p \frac{\partial T}{\partial t} = \left(V_{\mathrm{OCV}} - V_{\mathrm{cell}} - T \frac{\partial V_{\mathrm{OCV}}}{\partial T} \right) I - hA \left(T - T_{\mathrm{amb}} \right) \tag{6}$$

where the irreversible heat generation is expressed by

$$\left(V_{\mathrm{OCV}} - V_{\mathrm{cell}} \right) I \tag{7}$$

with V_{cell} being the full cell voltage, V_{OCV} being the cell Open Circuit Voltage (OCV) and I being the applied current. In our work, the convention is adopted that the sign of the applied current is positive during the discharge process and negative during the charging process. The reversible heat generation that is related to the cell's entropy, is given by the expression $TI\left(\partial V_{\mathrm{OCV}}/\partial T\right)$. The mean density of the cell's active material composites, the passive electric components, and its can is characterized by ρ. Its volume is given by V and the mean specific heat capacity is given by C_p, respectively. The convective heat exchange with the surroundings is described using the expression

$$hA \left(T - T_{\mathrm{amb}} \right) \tag{8}$$

where h is the heat-transfer coefficient, A is the intersectional area and T_{amb} is the ambient air temperature. The parameter set for the zero-dimensional thermal model is summarized in Table A.2.

2.2. Theoretical considerations

The polarization-based fast charging procedure we propose in this study is based on the findings of Liu [24], that suggest a correlation between the negative electrode's polarization and the risk of unwanted lithium plating. In their work, the authors found that the negative electrode's polarization, as well as the onset current for lithium plating, can be predicted by introducing an equivalent resistance. According to Liu [24], the introduced equivalent resistance summarizes the charge transfer resistance, the current collector/active particle contact resistance, and the resistance of the lithium-ion transport through the pores of the porous negative electrode. Liu [24] predicted the equivalent resistance via Electrochemical Impedance Spectroscopy (EIS) measurements from coin-type symmetrical cells that were built from the negative electrodes of dissembled single layer pouch cells. The authors subsequently calculated the negative electrode's polarization using the relation

$$\eta_{\mathrm{neg}} = R_{\mathrm{neg}} I \tag{9}$$

where R_{neg} is the introduced equivalent resistance and I is the full cell current. The interrelation between R_{neg} and the anode potential becomes prominent resolving Eq. (3) for $\Phi_s - \Phi_l$ at the anode-separator interface ($x = L_{\mathrm{neg}}$) according to

$$\Phi_{\mathrm{An,min}} = E_{\mathrm{eq,neg}}(x,t)\,|_{x=L_{\mathrm{neg}}} + \eta_{\mathrm{neg}}(x,t)\,|_{x=L_{\mathrm{neg}}} = E_{\mathrm{eq,neg}} + \eta_{\mathrm{neg}} \tag{10}$$

where $\Phi_{An,min}$ is the anode potential, $E_{\mathrm{eq,neg}}$ is the potential of the negative electrode in thermodynamic equilibrium and η_{neg} is the electrode's polarization. The negative electrode's potential in thermodynamic equilibrium is thereby calculated from the average lithium concentration within the porous electrode's active material [32]. As mentioned previously, Liu [24] found a negative correlation between the introduced equivalent resistance and the onset current for lithium plating using the outlined approach. This rather simple model is consequently found to be practicable for the prediction of the plating onset if the previously named resistances are the dominant factors determining when lithium plating occurs. However, the polarization due to lithium diffusion in the solid active material composite and the liquid electrolyte is neglected in the work of Liu [24]. According to the authors, this might hinder the practicability of the approach in diffusion limited systems with large active material composite particles or thick electrodes. It was furthermore not investigated, whether the relation is transferable from laboratory-format symmetrical cells to a technologically relevant (cylindrical or prismatic) battery format. Besides, the usability of the model for controlling a fast charging procedure has not yet been shown. In this regard, electrode heterogeneities resulting from high current rates might negatively influence the correlation between the negative electrode's polarization and the lithium plating onset. In this work, it is consequently investigated whether the approach introduced by Liu [24] is practicable for realizing an anode potential-controlled fast charging procedure in large-format lithium-ion batteries. The theoretical framework proposed by Liu [24] is therefore to be reformulated into a correlation between the full cell voltage and the anode potential, which indicates the lithium plating onset. The correlation between the full cell voltage and the anode potential is expected since the negative electrode's polarization directly contributes to the full cell polarization and the anode potential. This becomes prominent considering that the full cell polarization results from the sum of the positive and negative electrodes' polarization, the polarization of the insulating separator and the voltage drop induced by contact resistances, and the battery's passive electrical components [32]. It is given by

$$V_{\mathrm{cell}} - V_{\mathrm{OCV}} = \left(V_{\mathrm{pos}} - E_{\mathrm{eq,pos}} \right) - \left(V_{\mathrm{neg}} - E_{\mathrm{eq,neg}} \right) - R_{\mathrm{sep}} I - R_{\Omega} I \tag{11}$$

where V_{cell} is the full cell voltage and V_{OCV} is the battery's OCV. The expression $V_{\mathrm{pos/neg}} - E_{\mathrm{eq,pos/neg}}$ accounts for the deviation of the positive or negative electrode from its potential in thermodynamic equilibrium [32]. The voltage drop within the separator is given by $R_{\mathrm{sep}} I$, whereas the resistance of the battery's electrical components is accounted for by the expression $R_{\Omega} I$. The relation given in Eq. (11) accordingly reveals a linear contribution of the negative electrode's polarization to the full cell polarization, i.e. to the full cell voltage. The interrelation with the lithium plating reaction can be shown resolving the equation for the potential V_{neg} according to

$$V_{\mathrm{neg}} = -V_{\mathrm{cell}} + V_{\mathrm{OCV}} + E_{\mathrm{eq,neg}} + \left(V_{\mathrm{pos}} - E_{\mathrm{eq,pos}} \right) - R_{\mathrm{sep}} I - R_{\Omega} I \tag{12}$$

where V_{neg} according to Eq. (11) refers to the sum of the negative electrode's OCP and its polarization ($V_{\mathrm{neg}} = E_{\mathrm{eq,neg}} + \eta_{\mathrm{neg}}$). It is hence considered an electrode-averaged anode potential. The relation given in Eq. (12) consequently indicates that the contribution of the negative electrode's polarization to the full cell voltage translates into a relation of the form $V_{\mathrm{neg}} = a \cdot V_{\mathrm{cell}} + b$. The slope of the relation between the full cell voltage and the averaged anode potential is -1 which is in agreement with the work of Liu [24], in which a negative correlation between the negative electrode's polarization and the lithium plating onset was found. The x/y-intercept of the linear relation is simplified to $E_{\mathrm{eq,pos}}(T, \mathrm{SOC}) + \eta_{\mathrm{pos}}(I, T, \mathrm{SOC}) - R_{\mathrm{sep}} I - R_{\Omega} I$ if V_{OCV} is replaced by the difference of the positive and negative electrode's potentials in thermodynamic equilibrium ($E_{\mathrm{eq,pos}} - E_{\mathrm{eq,neg}}$). The relation for the simplified x/y-intercept of Eq. (12) suggests, that the positive electrode's potential in thermodynamic equilibrium, its polarization, and the voltage drop induced by the separator and the battery's electrical components negatively affect the correlation between the full cell voltage and the anode potential. The impact of the positive electrode's potential in thermodynamic equilibrium is thereby considered to be SOC- and temperature-dependent, while its polarization is assumed to depend on current, temperature and the battery's SOC. It is furthermore to be stressed that the anode potential is to be considered an area-dependent value [10,11,30]. The potential V_{neg} given in Eq. (12) in contrast is an electrode-averaged value which is considered to adequately reflect the lithium plating risk. The difference between V_{neg} and $\Phi_{\mathrm{An,min}}$ is formulated from Eqs. (10) and (12) as follows

$$V_{\mathrm{neg}} - \Phi_{\mathrm{An,min}} = \overline{E}_{\mathrm{eq,neg}} - E_{\mathrm{eq,neg}}\,|_{x=L_{\mathrm{neg}}} + \overline{\eta}_{\mathrm{neg}} - \eta_{\mathrm{neg}}\,|_{x=L_{\mathrm{neg}}} \tag{13}$$

where $\overline{E}_{\mathrm{eq,neg}}$ is the averaged potential of the negative electrode in thermodynamic equilibrium and $\overline{\eta}_{\mathrm{neg}}$ is the electrode-averaged polarization. The resulting relation states that differences between V_{neg} and the lithium plating onset, that is indicated by $\Phi_{An,min}$, are to be expected whenever the equilibrium potential and the polarization at the anode-separator interface ($x = L_{\mathrm{neg}}$) differs from the negative electrode's corresponding average values. The fact that electrode heterogeneities are expected to negatively influence correlation between cell voltage and anode potential might hinder the usability of the previously introduced relation for the realization of an anode potential-controlled fast charging procedure. The remaining part of this study, in consequence, aims to investigate whether the introduced approach is capable of predicting the lithium plating onset, despite of electrode heterogeneities and parasitically considered influences of the positive electrode and the insulating separator. Therefore, a correlation analysis is conducted, in which the relation between cell voltage is investigated under various operational conditions.

2.3. Correlation analysis

The relation between cell voltage and anode potential is subsequently analyzed by means of a simulation study in which we focus on two fundamental aspects: (i) the impact of the operational parameters and (ii) the influence of time-dependent processes (e.g. mass and charge transport in the solid active material and the liquid electrolyte). In this section, the simulations performed to analyze the previously outlined aspects are described. The corresponding results are discussed later on in this work. Regarding the impact of the operational parameters it is to be stressed, that a prominent influence of the prior charging current, the temperature profile or the initial SOC on the relation between cell voltage and anode potential would hinder its applicability in a fast charging procedure. The influence of time-dependent processes is investigated in order to assess whether there are negative influences on the usability of the relation for current/voltage regulation to be expected in a rather dynamic use case such as fast charging. This relates in particular to electrode heterogeneities that might negatively affect the validity of the relation under such conditions. The most relevant process in the context of unwanted lithium plating, i.e. mass transport in the liquid electrolyte, is assumed to have time-constants in the range of micro-seconds to minutes [33]. Therefore, the relation between cell voltage and anode potential is investigated in differential form, i.e. by means of $\partial V_{\mathrm{cell}}/\partial t$ and $\partial \Phi_{\mathrm{An,min}}/\partial t$, and at multiple time intervals after the cell is subjected to a highly frequent change in the charging current. The time-dependent nature of the electrochemical processes is however considered not to hinder the application of the relation between cell voltage and anode potential for the use in fast charging procedure, if there is no pronounced influence on the relation found.

Operational parameters.— During the correlation analysis, different current and temperature profiles are simulated. Thereby the influences of current and temperature on the correlation between cell voltage and anode potential are investigated separately. In the first set of simulations, the charging currents are regulated by means of a multi-step constant-current (MSCC) profile such that a current rate of 1C is reached in the final time-step of the simulation. The profile is thereby considered a function of the battery's SOC. The initial values are varied in 0.5C steps in a range between 0.5C and 2C. The number of steps in the charging profile is selected randomly from equally distributed values between 1 and 4. The battery temperature is kept constant at 25 °C. In a second set of simulations, the initial temperature is varied in 5 K steps in the range between 15 °C and 35 °C, while the current is kept at a constant rate of 1C. The battery temperature is likewise controlled in such way that a predefined value of 25 °C is reached in the final simulation time-step. It is noteworthy that the applied temperature profiles were generically specified and do not aim for most accurately simulating the battery's temperature behavior. Instead, simplified profiles with constantly increasing or decreasing temperature

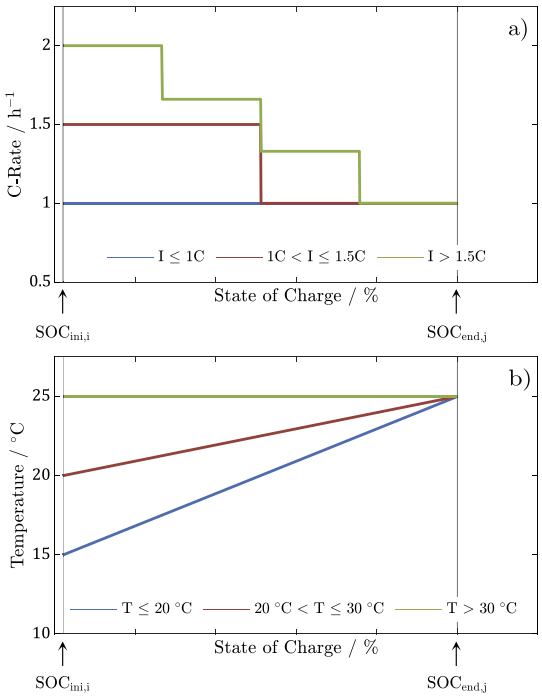

Fig. 1. Exemplary current profiles (a) and temperature profiles (b) applied in simulations performed in order to investigate the relation between cell voltage and anode potential and its dependency on the previous charging procedure. The initial charging state $\mathrm{SOC_{ini}}$ is varied, and the relation is investigated in a predefined charging state $\mathrm{SOC_{end}}$.

were chosen. These profiles are considered sufficient for the purpose of this study although they do not represent the thermal behavior expected for lithium-ion batteries in fast charging applications. In addition to the temperature and current variations, the initial SOC is varied stochastically assuming equally distributed values between 0% SOC and 50% SOC. Exemplary current and temperature profiles corresponding to the outlined simulation sets are shown in Fig. 1(a) and (b). The relation between cell voltage and anode potential is investigated in the final time-step of the simulation for both simulation sets, where current rate, temperature and the SOC are identical (1C, 25 °C, and 50%) for all simulated profiles. Note, that the system is due to the applied current considered not to be in thermodynamic equilibrium in the respective time-step. Table 1 summarizes the operational parameters of the simulation cases in the outlined first part of this study.

The previously outlined procedure aims to evaluate whether a distinct correlation between cell voltage and anode potential is found under predefined operational conditions, independently of current rate and temperature during the previous charging procedure, and the initial SOC. Whether a similar correlation can be found in various operational conditions is investigated in a second simulation study. Thereby, multiple current rates, temperatures and end-of-charge SOCs are examined. During the corresponding simulations, the current and temperature profiles, as well as the initial SOC are varied stochastically similar to the previously described procedure. The initial current rate is again varied in 0.5C steps in a range between 0.5C and 2C and temperature is varied applying initial values between 15 °C and 35 °C in steps of 5 K. In contrast to the previous simulation sets, the influences of current rate and temperature are varied in a multivariant analysis, i.e., the impact of the respective measures are not evaluated separately this time. The applied current and temperature profiles are regulated in such way that predefined current rates, SOCs and temperatures are reached at the end of the simulation. Thereby, current rates of 1.5C, 1.3C and 1C are investigated at and end-of-charge temperature of 25

Table 1
Initial current, temperature and state of charge for simulation cases in the analysis of the correlation between cell voltage and anode potential.

	Sim. Set 1	Sim. Set 2
Current profile		
I_{ini}	[0.5 C 2 C]	1C
I_{end}	1C	1C
Temperature profile		
T_{ini}	25 °C	[15 °C 35 °C]
T_{end}	25 °C	25 °C
Charging state		
SOC_{ini}	[0% SOC_{end}]	[0% SOC_{end}]
SOC_{end}	50%	50%

Table 2
Initial current, temperature, and SOC as well as operational parameters at the end-of-charge SOC for simulation cases in the analysis of the correlation between cell voltage and anode potential.

	Sim. Set 1	Sim. Set 2	Sim. Set 3
Current profile			
I_{ini}	[0.5C 2C]	[0.5C 2C]	[0.5C 2C]
I_{end}	1C, 1.3C, 1.5C	1C	1C
Temperature profile			
T_{ini}	[15 °C 35 °C]	[15 °C 35 °C]	[15 °C 35 °C]
T_{end}	25 °C	15 °C 25 °C 35 °C	25 °C
Charging state			
SOC_{ini}	[0% SOC_{end}]	[0% SOC_{end}]	[0% SOC_{end}]
SOC_{end}	50%	50%	30%, 40%, 50%

°C and a final SOC of 50%. Regarding temperature, three different end-of-charge values of 15 °C, 25 °C and 35 °C are analyzed at a current rate of 1C and at 50% SOC. The correlation is furthermore evaluated at three different end-of-charge SOCs, namely 30%, 40% and 50% at a current rate of 1C and a temperature of 25 °C. Table 2 summarizes the operational parameters for the outlined investigations as part of the correlation analysis.

Differential behavior.— The approach used to analyze the practicability of the correlation for fast charging in a dynamic battery state is described in the following subsection. Thereby, a general two-step current profile is used as shown in Fig. 2(a). During the simulation set, the initial current I_{ini} as well as the current difference $\Delta I_{j-1,j}$ between the first current step I_{j-1} and the second current step I_j are varied randomly assuming a uniform distribution. The subscript j thereby represents the number of current steps in the respective profile. The step in the current profile is applied at different SOCs (10%, 30% and 50%). The simulations are performed at different temperatures that are varied randomly from equally distributed values in the range between 15 °C and 35 °C. It is however to be stressed, that the battery temperature, even though it is varied between the simulations, is kept constant throughout one particular simulation. Hence, an isothermal behavior of the battery is assumed. This approach allows for investigating the correlation between cell voltage and anode potential at various current rates neglecting the influence of the respective current on the battery's temperature. Table 3 summarizes the simulation parameters, i.e. initial current rate, current difference between the first and second current step, temperature and the SOC at the time step t_1 at which the charging current is changed from I_{j-1} to I_j. The differences in cell voltage and anode potential are analyzed in three different time intervals Δt of 30 s, 90 s and 180 s after the current step as shown in Fig. 2(b) and (c). The differences are calculated according to

$$\frac{\partial V_{cell}}{\partial t} := \frac{\Delta V_{cell}}{\Delta t} = \frac{V_{cell}(t_2) - V_{cell}(t_1)}{t_2 - t_1} \tag{14}$$

and

$$\frac{\partial \Phi_{An,min}}{\partial t} := \frac{\Delta \Phi_{An,min}}{\Delta t} = \frac{\Phi_{An,min}(t_2) - \Phi_{An,min}(t_1)}{t_2 - t_1} \tag{15}$$

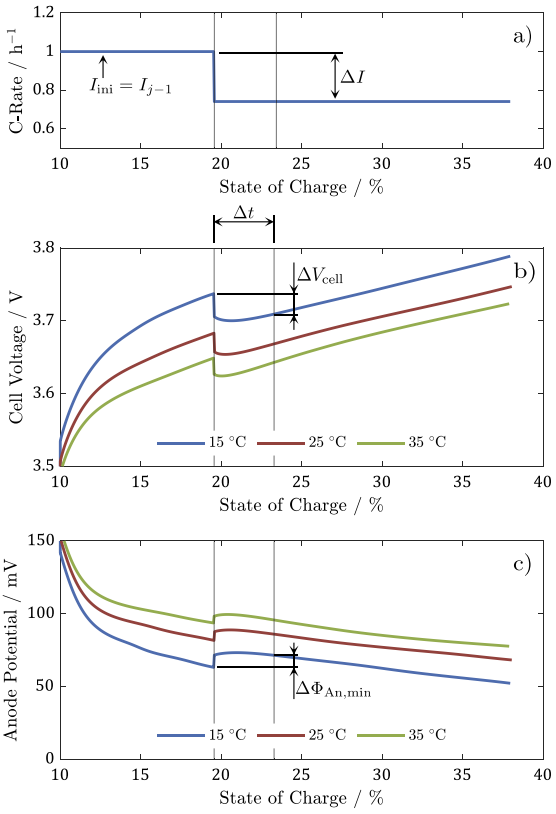

Fig. 2. Method used to investigate the correlation between differences in cell voltage and anode potential following a step in the applied current profile. The corresponding two-step current profile is exemplary shown in (a). The resulting cell voltage and anode potential profiles are shown in (b) and (c). The differences in cell voltage and anode potential are highlighted for on exemplary time interval.

Table 3
Initial current, current step, temperature and SOC at the time-step at which the charging current is varied for simulation cases used to analyze the correlation between differences in cell voltage and anode potential.

	Sim. Set 1	Sim. Set 2	Sim. Set 3
Current profile			
I_{ini}	[0.5C 2C]	1C	1C
$\Delta I = I_{j-1} - I_j$	0.3C	[0.1C 0.5C]	1C
Temperature profile			
T = const.	[15 °C 35 °C]	[15 °C 35 °C]	[15 °C 35 °C]
Charging state			
SOC (t_1)	50%	50%	10%, 30%, 50%

where ΔV_{cell} is the full cell voltage difference and $\Delta \Phi_{An,min}$ is the change in the anode potential. The time interval at which the differences in cell voltage and anode are investigated is characterized by t_1 and t_2, respectively. As can be obtained from Eqs. (14) and (15), the time-dependent gradient of both measures, cell voltage and anode potential, is approximated linearly.

2.4. Novel fast charging procedure

The results of the previously outlined correlation analysis are used for the implementation of a polarization-based fast charging procedure. Thereby, a voltage threshold is derived from the relation between cell voltage and anode potential. The voltage threshold is subsequently used for a voltage regulation in the proposed fast charging procedure. It is considered to correlate with the lithium plating onset. The polarization-based procedure is, due to the use of the correlation, considered capable

of avoiding lithium plating. This section aims to describe the procedure used to derive the voltage threshold. Thereafter, a possible implementation of the novel fast charging procedure is described. Fig. 3 illustrates the procedure used to derive the voltage threshold as well as an exemplary fast charging procedure according to the polarization-based approach we propose.

Derivation of voltage threshold.— The voltage threshold is derived by means of multiple CC charging simulations. The simulations are terminated as soon as the anode potential target value, indicated by the expression $(\boldsymbol{\Phi}_s - \boldsymbol{\Phi}_l)_{\text{target}}$, is reached. Fig. 3(a) and (b) show the corresponding cell voltage and anode potential profiles resulting for three different current rates of 1C, 1.5C, and 2C and a constant temperature of 25 °C. However, simulations are performed with (constant) charging currents in a wide range between 0.3C and 2.5C to derive the voltage threshold applied in the proposed fast charging procedure. The maximum current rate of 2.5C is thereby adopted from the cell manufacturer's recommendations for the cell investigated in this work. The target anode potential value is to be defined in such way that lithium plating is avoided. In this work, an anode potential buffer value ΔV of 10 mV with respect to the theoretical onset condition of the lithium plating reaction, i.e. 0 V vs. Li/Li$^+$, is defined. The respective value of 10 mV is in accordance with literature [12,13]. The buffer value is considered to account for inhomogeneities such as current and polarization inhomogeneities along the current collecting foils [28,29,34,35]. Due to the correlation between cell voltage and anode potential, the cell voltage values shown in Fig. 3(b) are considered to correlate with the anode potential target value. This is indicated in Fig. 3 using the expression corr$(V, \boldsymbol{\Phi})$. The simulations are furthermore conducted at different temperatures between 15 °C and 60 °C. In consequence, voltage thresholds are determined for various temperatures to most accurately reproduce the battery behavior at different temperatures.

Polarization-based fast charging procedure.— The voltage threshold, which is used for voltage regulation in the polarization-based fast charging procedure is shown in Fig. 3(c). It is, due to the correlation between cell voltage and anode potential assumed, that for a particular SOC, voltages below the threshold do not result in an anode potential below 10 mV. Thus, lithium plating should not occur as long as the full cell voltage does not exceed the introduced threshold value. This assumption can be explained by the fact that, at a predefined SOC, lower cell voltages correspond to a reduced polarization of both the negative electrode and the full cell. The reduced polarization of the negative electrode reduces the risk of lithium plating according to the expression given in Eq. (10). The proposed procedure subsequently allows for applying a higher current rate whenever the measured/simulated full cell voltage is lower than the voltage threshold specified previously. This is possible regardless of the battery's temperature, its SOC or the operational parameters throughout the previous charging procedure. The implementation of the voltage regulation as part of the fast charging procedure is to be explained in detail as follows: In our example, the fast charging procedure is initiated with a CC phase at 1.5C that is applied until the voltage threshold is reached for the first time. It is thereby to be taken into consideration, that the battery is in thermodynamic equilibrium prior to the charging process. The cell full cell voltage is accordingly well below the predefined voltage threshold. The subsequent second phase of the fast charging procedure is characterized by a voltage-regulated charging process in which the voltage threshold is used as a reference for the feedback-control. The voltage regulation is implemented using a PI-controller. The controller setup is outlined in Appendix B. During the voltage-controlled phase, the current rate decreases monotonously. The anode potential is intended to be kept constant at the previously specified target value of 10 mV vs. Li/Li$^+$ in this phase. The voltage-controlled phase is hence considered an anode potential controlled phase. However, model limitations, the quality of the cell voltage measurement or inaccuracies in the voltage regulation might cause deviations from the anode potential target value. Additionally, electrode heterogeneities and parasitically considered influences

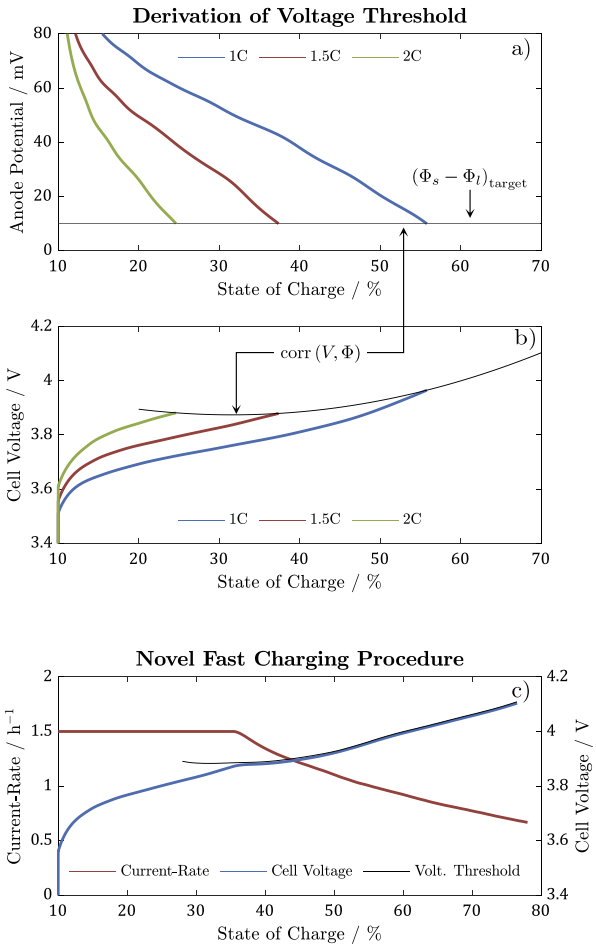

Fig. 3. Derivation of voltage threshold by means of constant-current charging simulations with three different current rates of 1C, 1.5C and 2C that are terminated when the anode potential target value $(\boldsymbol{\Phi}_s - \boldsymbol{\Phi}_l)_{\text{target}}$ is reached as shown in (a). The threshold results from assigning the resulting cell voltage values to the corresponding SOC. Due to the correlation between cell voltage and anode potential, the resulting voltage curve that is shown in (b) is considered to correlate with the anode potential target value. This is indicated in (a) and (b) using the expression corr $(V, \boldsymbol{\Phi})$. The threshold is used for a voltage-regulated phase in the novel fast charging procedure proposed in this study. The respective phase begins as soon as the measured full cell voltage information reaches the voltage threshold for the first time as shown in (c).

of the positive electrode and the separator might hinder the procedure to control the anode potential sufficiently accurate. Whether the proposed fast charging procedure is nevertheless capable of avoiding the lithium plating reaction is investigated in detail in Section 3. The polarization-based procedure is, due to the implemented anode potential regulation in the voltage-controlled phase, considered to be advantageous especially in the event of unforeseen changes in the operational boundary conditions, i.e. variations in the initial current rate or subsequent variations in temperature due to changes in the available cooling power. This is likewise to be demonstrated later on in this study by comparing the proposed polarization-based procedure to recently introduced fast charge algorithms [12,13] by means of the minimum anode potential and charging time at varying boundary conditions.

3. Results and discussion

3.1. Anode potential characteristics analysis

Operational parameters.— In the following subsection, the results of the previously described simulation studies are discussed. It is thereby

to be evaluated whether a correlation between cell voltage and anode potential is to be found on a full cell level. The full cell voltage and the anode potential are thereby investigated at a predefined set of operational conditions (1C, 25 °C, and 50% SOC). Due to the application of the generic current and temperature profiles shown in Fig. 1, the specified operational conditions are reached in the final simulation time-step, as was described previously. The initial values of current, temperature as well as the initial SOC are varied according to Table 1. In summary, a total number of 100 simulations with varying initial conditions are performed. The results of the respective simulations sets are shown separately for current and temperature in Fig. 4. Thereby, an approximately linear correlation between cell voltage and anode potential is found. The previously described variations in current and temperature as well as in the initial SOC are not found to considerably affect the correlation as shown in Fig. 4(a) and (b). Nevertheless, there is a shift towards higher cell voltages observable when the initial current rate is increased from 0.5C to 2C and when the initial temperature is reduced from 35 °C to 15 °C. This is indicated in Fig. 4 by means of (dashed) trend lines for the respective currents and temperatures. The observed shifts are attributed to the parasitically considered influences of the positive electrode, the separator and the battery's electrical components, that are, according to Eq. (12), expected to cause changes in the x/y-intersect. In addition to the observed cell voltage shifts, the slope of the trend lines is found to vary, when current and temperature are varied. This is to be explained by inhomogeneities in the negative electrode that are found to increase with decreasing cell voltage as indicated in Fig. 4. The increasing electrode-heterogeneities are attributed to variations in the initial SOC. Thereby, an inhomogeneous distribution of lithium-ions in the solid active material phase and the liquid electrolyte, which is observed for high initial charging states, is considered to result from transport limitations [33].

The fact that a distinct correlation is found between cell voltage and anode potential and that this relation is not significantly affected by the operational conditions of the previous charging procedure suggests that the approach introduced by Liu [24] might be transferable to the full cell level. Accordingly, the onset for lithium plating is assumed to be predictable from the full cell polarization. It is however to be stressed, that up to this point, only a predefined set of operational conditions was investigated. The utilization in a polarization-based fast charging procedure however requires the correlation likewise to be found under various operational parameters. The correlation is therefore to be investigated at different end-of-charge current rates, temperatures, and SOCs. The corresponding simulations are part of the second simulation study that is performed in our work (See Table 2). The results of the correlation analysis are shown in Fig. 5. The Figure shows the cell voltage and anode potential values resulting for three different current rates I_{end} between 1C and 1.5C, three different temperatures T_{end} between 15 °C and 35 °C, and three different end-of-charge SOCs between 30% and 50%. During the investigations, the charging profile, the temperature profile as well as the initial SOC are varied randomly. Note that the results are not analyzed separately for current and temperature variation as previously. This is due to the fact that current and temperature variations were not found to considerably influence the correlation under the operational conditions investigated earlier (See Fig. 4). As shown in Fig. 5, an approximately linear relation is found for all operational conditions investigated. There is however an influence of current, temperature and the end-of-charge SOC observable. The simulation results are subsequently shifted towards higher cell voltages and lower anode potentials when increasing the current rate from 1C to 1.5C. This is shown in Fig. 5(a), (b) and (c). A similar behavior is observed when decreasing the temperature from 35 °C to 15 °C as shown in Fig. 5(d), (e) and (f). In general, a shift in the simulation results is considered to indicate an increase or decrease in the polarization of the negative electrode and the full cell. An increased polarization (i.e. a shift towards higher cell voltages) is for instance expected when increasing the current rate or reducing the temperature [36,37]. The

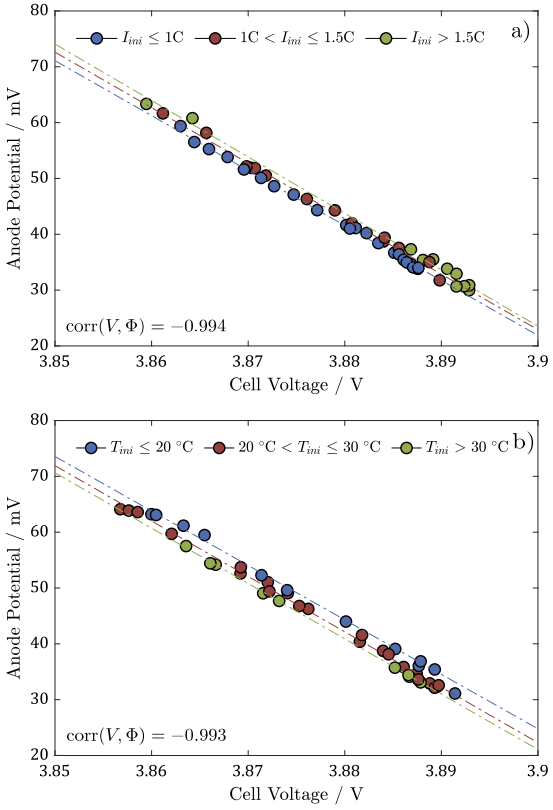

Fig. 4. Correlation between cell voltage and anode potential at predefined operational parameters of 1C, 25 °C and 50% SOC. Current (a) and temperature (b) are regulated in such way that a current rate of 1C and a temperature of 25 °C are reached precisely at 50% SOC. The initial values of current and temperature as well as the initial SOC is varied randomly assuming uniformly distributed values. Throughout the simulations with current variation (a), the temperature is kept at a constant value of 25 °C. Likewise, the current rate is kept constantly at 1C throughout the simulations with varying temperature profiles (b).

linear relations shown in Fig. 5 are moreover found to have varying gradients for different current rates and temperatures. Thereby, a trend is to be observed for an increased current rate or a reduced temperature in the final simulation time-step. The gradient decreases when the end-of-charge current is increased from 1C to 1.5C or when the temperature in the final simulation time-step is reduced from 35 °C to 15 °C. The changes in the slope of the linear relation are to be explained by electrode-heterogeneities that are considered to be most pronounced for high charging rates and low temperatures. The contribution of the positive electrode, the insulating separator, and the battery's electrical components to V_{neg} is likewise interpreted as a change in the slope. Regarding the battery's SOC, a shift in the simulation results towards higher cell voltages and lower anode potentials is found when increasing the end-of-charge SOC as shown in Fig. 5(g), (h) and (i). The observed shift in cell voltage is in this context explained by the SOC-dependency of the OCV and the negative electrode's potential in thermodynamic equilibrium. This is due to the fact, that the full cell polarization as well as the negative electrode's polarization are not considered to vary significantly when varying the end-of-charge SOC. The electrode's potential in thermodynamic equilibrium in contrast shows a clear dependency on the charging state resulting in variations of the anode potential. Due to the fact that the correlation between cell voltage and anode potential remains distinctive (and linear) even under varying operational parameters, its usability for an anode potential controlled fast charging procedure is not considered to be limited to certain current rates, temperatures or SOC ranges. Nevertheless, an impact on the accuracy of the anode potential regulation is expected

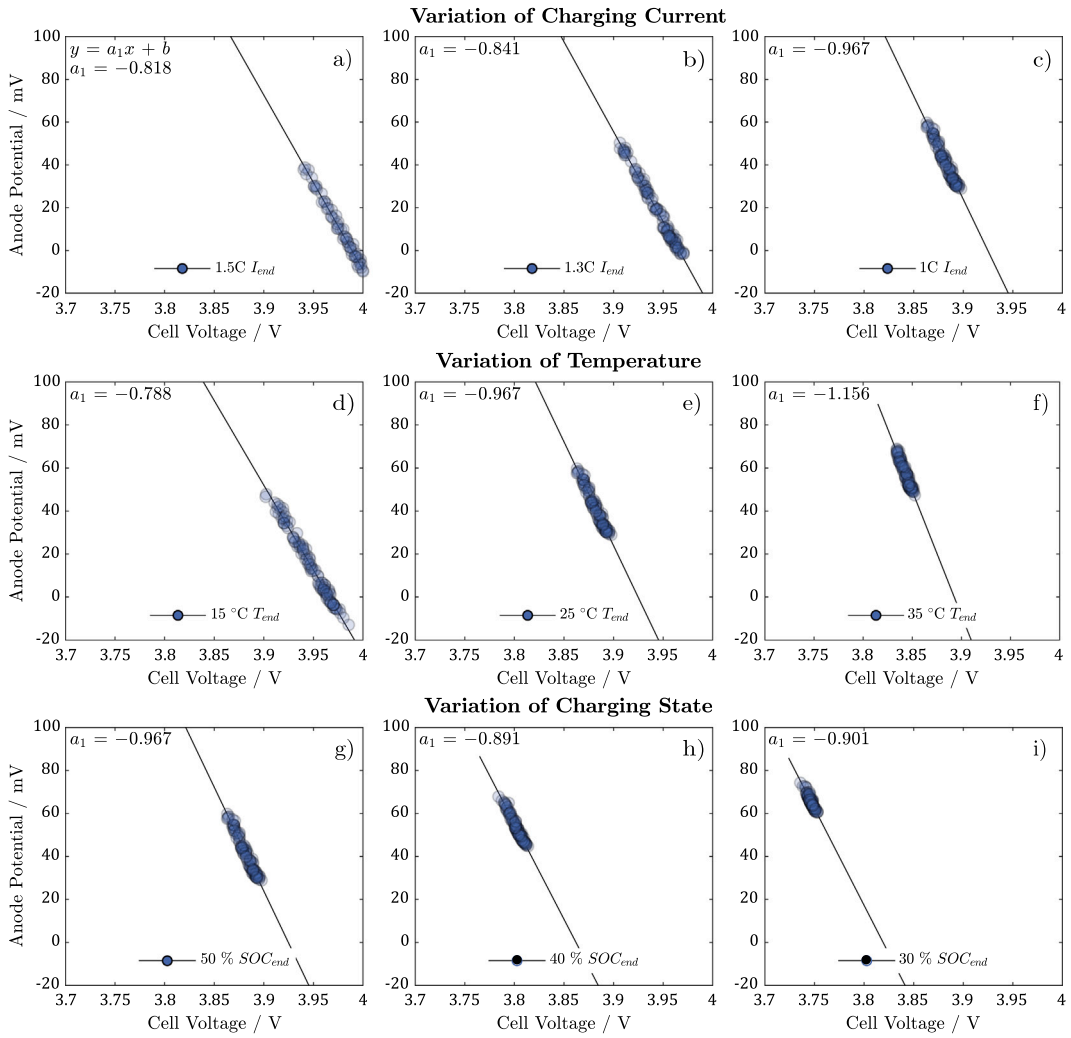

Fig. 5. Correlation between cell voltage and anode potential at different operational parameters of the battery cell. The operational parameters are varied in ranges between 1.5C and 1C for the end-of-charge current rate (a), (b) and (c), between 15 °C and 35 °C for end-of-charge temperature (d), (e) and (f), and between 50% SOC and 30% SOC for end-of-charge SOC (g), (h) and (i). Initial values of current, temperature and SOC are varied randomly assuming uniformly distributed values. The gradient of the trend line, which is highlighted in the Figure using the parameter a1 following the general linear equation $y = a_1 x + b$, indicates the inaccuracy in an anode potential regulation in mV when a 1 mV error in the measurement of cell voltage is assumed.

due to the observed variations in the gradient of the linear fit. This is to be explained by means of a general linear equation following the convention $y = a_1 \cdot x + b$. The cell voltage is thereby represented by the variable x. The resulting inaccuracy in the anode potential y is subsequently to be predicted by means of the gradient a_1 of the linear fit. Thereby, an increasing gradient causes the anode potential regulation's inaccuracy to be increased. The changes in the trend line's gradient observed when reducing the initial current rate from 1.5C to 1C for instance results in an increase of the inaccuracy from 8.2 mV to 9.6 mV assuming an error in cell voltage measurement of 10 mV. Likewise, the inaccuracy in anode potential regulation is expected to increase from 7.9 mV to 11.2 mV when increasing the end-of-charge temperature from 15 °C to 35 °C. The proposed fast charging procedure is accordingly expected to show best accuracies for high current rates up to 2.5C and low temperatures of 15 °C. This is in accordance with the work of Jow [38], stating that the battery's resistance is dominated by the anode resistance at low temperatures.

Differential behavior.— Regarding the relation between the $\partial V_{\text{cell}}/\partial t$ and $\partial \Phi_{\text{An,min}}/\partial t$, differences in cell voltage and anode potential, after applying a two-step current profile, are to be investigated. Thereby, the initial current rate I_1, the current step $\Delta I_{2,1}$, the temperature T, and the SOC at the switching point in the current profile SOC (t_1) are varied. The correlation is investigated at three different time intervals Δt of 30 s, 90 s and 180 s after the switching point in the current profile. Fig. 6 shows the results grouped by initial current rate, current step, and the SOC at the switching point. The corresponding simulation parameters are summarized in Table 3. During the analysis, a linear correlation is found for all operational parameters that were investigated. There is however an influence of the initial current rate, the current step and the SOC at the switching point in the two-step CC profile observable. The quality of the correlation is in this regard quantified by means of the Pearson coefficient. It is shown in Fig. 6(a) and (d), that variations of the initial current rate, and the current step between the two phases of the applied profile show most prominent influences after a time span of 30 s. The correlation coefficient however shows increasing values for 90 s and 180 s. This behavior is to be explained by differently pronounced electrode-heterogeneities expected for different initial current rates and different current steps that are balanced out with increasing Δt. The influence of the SOC on the correlation is to be attributed to variations in the slopes of the negative and positive electrodes' potentials in thermodynamic equilibrium. In addition, the battery's SOC-dependent internal resistance is expected to have an impact on the behavior of the correlation. This is expected most prominently at charging states below 10% SOC where increased resistances are reported [37]. However, the analysis of the positive and negative electrodes' equilibrium potentials and their polarizations influence on the correlation is out of scope

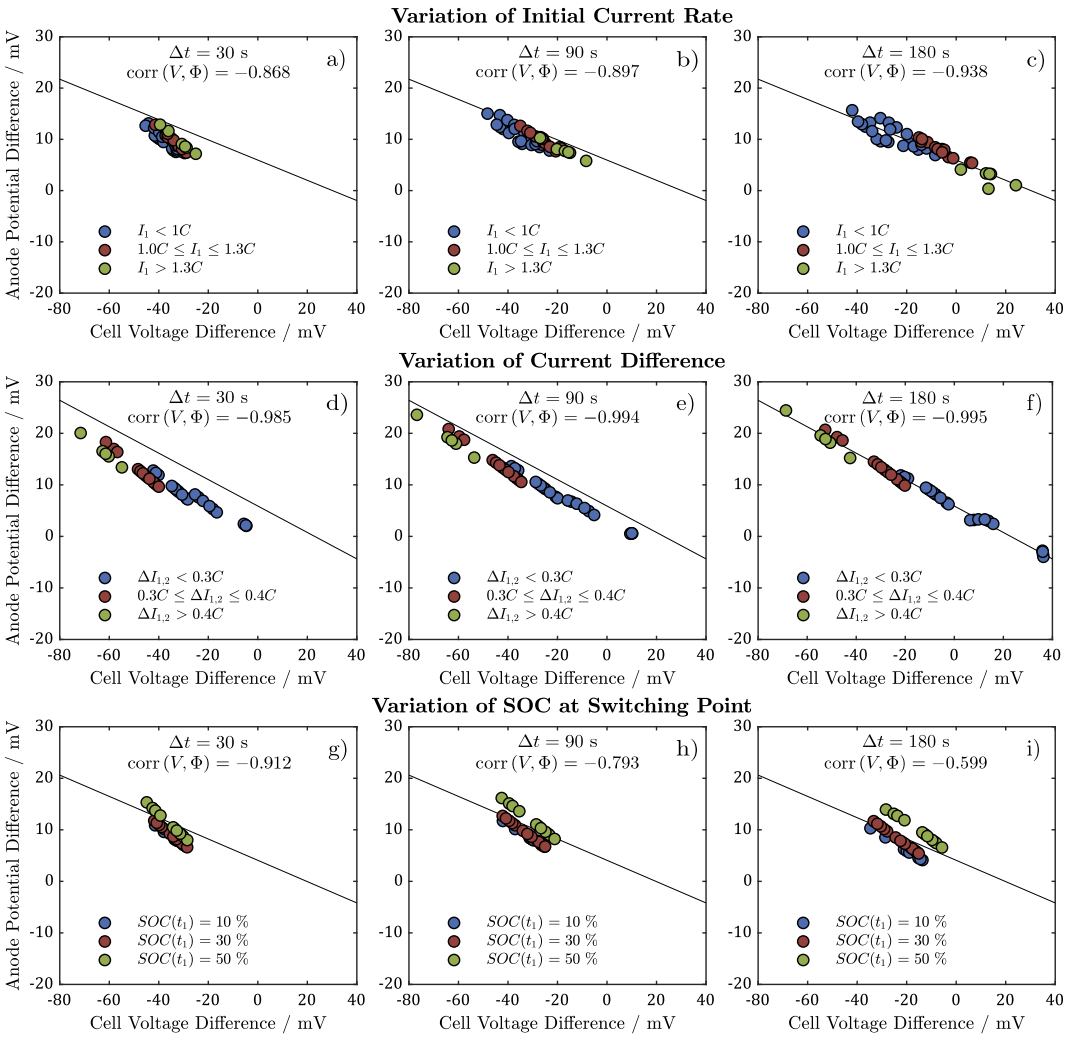

Fig. 6. Correlation between $\partial V_{\text{cell}}/\partial t$ and $\partial \Phi_{\text{An,min}}/\partial t$ investigated applying two-step CC current profiles with varying initial current rates (a), (b), and (c), varying current steps between the first and the second step of the applied current profile (d), (e) and (f) and varying SOCs at the switching point in the current profile (g), (h) and (i). Multiple data points of the same color result for different temperatures at which the correlation between $\partial V_{\text{cell}}/\partial t$ and $\partial \Phi_{\text{An,min}}/\partial t$ is investigated. (For interpretation of the references to color in this figure legend, the reader is referred to the web version of this article.)

for this study. The various effects are therefore not separated for the illustration in Fig. 6. The results shown in Fig. 6(a)–(f) nevertheless suggest, that the most prominent changes in the polarization affecting the correlation between differences in cell voltage and anode potential decay within 180 s. These results are well in line with the finding of Jossen [33], suggesting that the correlation between differences in cell voltage and anode potential is suitable for predicting the gradient of the anode potential under the assumption of a steady-state battery state. The computational extensive Newman-type P2D model is thereby not necessarily to be implemented in the control algorithm. However, the fact that the correlations validity is found to be limited to steady-states is considered a distinctive constraint for the usability in fast charging procedures.

3.2. Polarization-based fast charging procedure

The practicability of the polarization-based approach for the implementation of an anode potential regulated fast charging procedure is to be demonstrated by means of simulation in the subsequent subsection. The previously outlined results of the correlation analysis are thereby considered a strong indicator for the feasibility of the relation between cell voltage and anode potential to predict the lithium plating risk in a technologically relevant battery format. However, the dependency of the introduced voltage threshold on the operational conditions (current, temperature and the initial SOC) are yet to be investigated. This section consequently aims to derive voltage threshold for different maximum current rates between 1C and 2C, various temperature of 15 °C, 25 °C and 35 °C and various initial charging states of 10% SOC, 30% SOC and 50% SOC. The anode potential target value is specified to be 10 mV vs. Li/Li$^+$ in the CC charging simulations used to determine the current, temperature, and SOC dependent thresholds. The buffer value ΔV of 10 mV with respect to the theoretical onset for unwanted lithium plating is considered to account for inhomogeneities of temperature, local potentials as mentioned previously. The derived voltage thresholds are subsequently used to control the fast charging process in two exemplary use cases with different current boundary conditions. It is thereby to be evaluated whether the anode potential is controlled sufficiently accurate at its target value using the proposed procedure.

Derivation of voltage reference curve.— The voltage thresholds, which are derived by means CC charging simulations for different maximum current rates, temperatures, and initial SOCs, are shown in Fig. 7. Note, that the maximum current rate of 2.5C, that was adopted from the battery manufacturer's specifications, is not exceeded. The maximum charging current is furthermore limited to 1C, 1.5C and 2C to investigate the threshold's dependency on the maximum applied current rate,

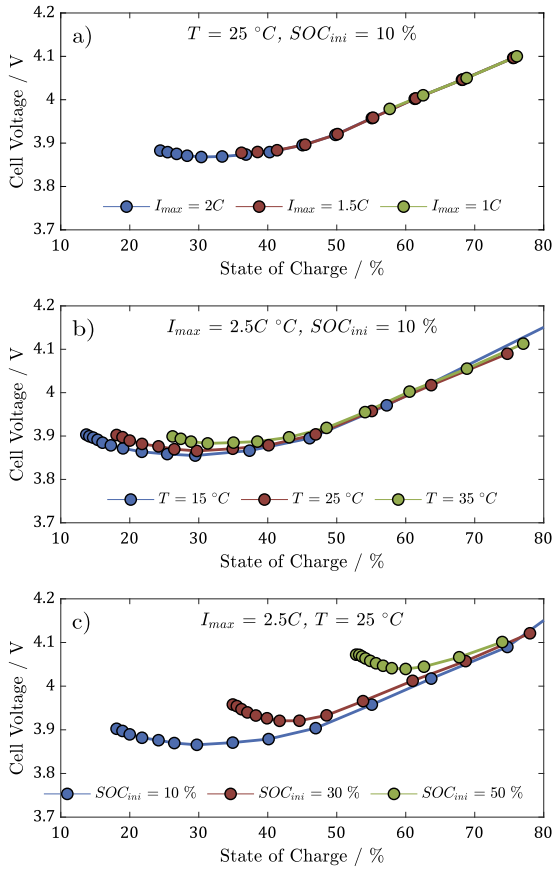

Fig. 7. Voltage thresholds for different maximum current rates of 1C, 1.5C and 2C (a), for different (isothermal) temperatures of 15 °C, 25 °C and 35 °C (b) and for different initial charging states of 10% SOC, 30% SOC and 50% SOC (c). During the variation of the maximum current rate and the initial SOC, temperature was kept at a constant value of 25 °C. Likewise, the maximum current rate was kept constant at 2.5C for the investigation of different temperatures and initial SOCs. The initial charging state is similarly kept constant at 10% SOC whenever current rate and temperature are varied. Multiple data points of one color represent simulations at different initial current rates considering that the voltage thresholds are derived by means of CC simulations with various current rates. (For interpretation of the references to color in this figure legend, the reader is referred to the web version of this article.)

as shown in Fig. 7(a). As shown in Fig. 7, the voltage thresholds are generally observed to show a rather linear shape in wide SOC ranges. This is well in line with the work of Mai [12] in which the simulated cell voltage in an anode potential controlled fast charging procedure was approximated by a linear-shaped voltage ramp. However, the reference voltage curves are found to show a non-linear region at the leftmost segment of each individual graph. The non-linear region expands furthermost for high current rates, low temperatures and for a low initial charging state of 10% SOC. It is however not to be observed for a maximum current rate of 1C as shown in Fig. 7(a). The observed influences suggest an interrelation with the polarization of both the negative electrode and the full cell. However, further investigating the battery's polarization would exceed the scope of this work. A detailed analysis of the positive and negative electrodes' polarizations following the approach introduced by Nyman [32] is hence to be found in the supplementary material of this work. It is to be stressed, that the non-linear behavior of the voltage threshold and the observed dependency on temperature and the initial SOC are not considered constraints for the proposed polarization-based fast charging algorithm.

Polarization-based fast charging procedure.— The previously described polarization-based fast charging procedure is subsequently to be validated by means of simulation. Thereby, two initial current rates of 2C and 1.5C are investigated. The battery's temperature is kept at 25 °C throughout the entire charging procedure assuming isothermal battery behavior. The initial SOC is specified to be as high as 10% and the battery is intended to be charged to 80% SOC. The results of the respective simulations are shown in Fig. 8. Thereby, the current profile, the full cell voltage, the reference voltage curve, and the anode potential are shown in Fig. 8(a) for an initial current rate as high as 2C and in Fig. 8(b) for an initial current rate as high as 1.5C. Due to the fact that temperature was kept constant throughout the simulations, it is not shown in Fig. 8. Identical voltage thresholds are used for both simulations, taking into consideration that the voltage reference curve was not found to show a distinct dependency on the maximum current rate (See Fig. 7(a)). The cell voltage initially shows values well below the predefined voltage threshold allowing for CC phases at 2C and 1.5C as shown in Fig. 8(a) and (b). The initial CC phase is thereby found to be considerably longer for an initial current rate of 1.5C compared to an initial current rate of 2C. This is due to the lower polarization expected for a reduced current rate causing the full cell voltage to reach the voltage threshold at a higher charging state. As shown in the lower parts of Fig. 8(a) and (b), the anode potential is regulated with an accuracy of ±2 mV using the previously derived voltage threshold as a reference in the voltage-controlled phase. The observed inaccuracy is found to be most prominent when switching from the initial CC phase to the voltage-controlled phase and is caused by a non-ideally parameterized PI-controller. This becomes particularly prominent taking into account that the full cell voltage marginally exceeds the voltage threshold between 24% and 30% SOC, i.e. in the initial phase of the voltage regulation, in the simulation with a maximum current rate of 2C. The corresponding SOC range is highlighted in Fig. 8(a). It is furthermore to be found that decreasing the maximum applied current rate from 2C to 1.5C causes the inaccuracy to be reduced. This is likewise considered an indicator for a non-ideally parameterized controller. The introduced voltage curves derived from the polarization-induced correlation between cell voltage and anode potential are subsequently found to be practicable to predict the likelihood of the unwanted plating reaction during fast charging. Its validity for preventing the lithium plating phenomena is demonstrated independently of the phase of the charging procedure and the operational parameters.

3.3. Current control under varying boundary conditions

The subsequent section aims to discuss the benefits of the polarization-based fast charging procedure expected most notably under varying boundary conditions (e.g. current and temperature). The performance of the algorithm under such conditions is therefore compared to that of the fast charging approaches recently introduced by Mai [12] and Sieg [13] by means of the minimum anode potential throughout the charging process. The minimum anode potential is in this regard considered to represent the onset of lithium plating. The polarization based procedure is furthermore compared to the mentioned approaches in terms of the accuracy of the anode potential regulation. The accuracy of the regulation is to be evaluated by means of the Root Mean Square Error (RMSE) of the anode potential with respect to the target value of 10 mV vs. Li/Li^+. The reference charging process for the comparison is specified to be a fast charging procedure from 10% to 80% SOC at a maximum current rate of 2.5C and an ambient temperature of 25 °C. These respective conditions are referred to as 'Case 01' in the subsequent discussion. In order to investigate the performance of the fast charging procedures under a varying temperature boundary condition, the ambient temperature is reduced to 15 °C. The maximum current rate remains at 2.5C and the initial charging state is maintained at 10% SOC. The corresponding boundary conditions are referred to as 'Case 02' in the following subsections. The current limitations described previously are simulated by reducing the current rate to 1C for the first 10 min of the charging procedure. The ambient temperatures is kept constant at 25 °C and the initial charging

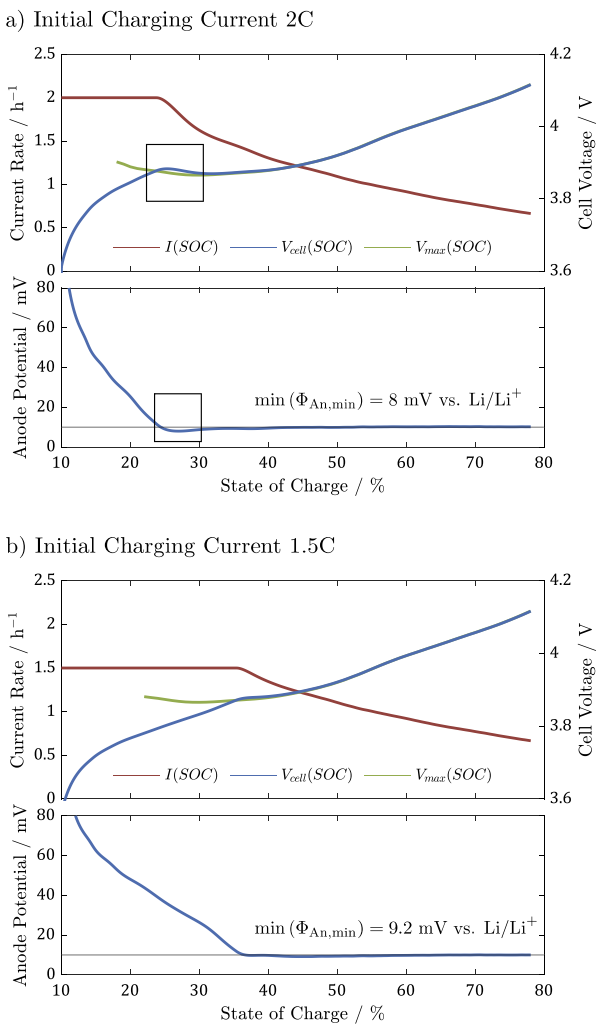

Fig. 8. Validation of the proposed method utilizing the previously discussed reference voltage curves as threshold for voltage regulation. For this purpose, two fast charging procedures with maximum current rates of 2C (a) and 1.5C (b) are simulated. Temperature is kept constant at 25 °C throughout the charging simulations and is consequently not shown. The initial charging state is specified to be 10% SOC. The charging procedure is thereby subdivided into an initial CC phase and a successive voltage controlled phase. Marginal deviations of the anode potential target value due to a non-ideally parameterized PI controller are highlighted in (a).

state is kept at 10% SOC. The simulation use case corresponding to the infrastructural current limitation is hereafter referred to as 'Case 03'. It is to be stressed that, in the corresponding simulation sets 'Case 01–03', the battery's temperature is modeled using the 0D thermal model outlined earlier in this work. Accordingly, the influence of temperature variations during fast charging is taken into consideration when comparing the polarization-based procedure to fast charging procedures adopted from the literature [12,13]. The voltage-based approach introduced by Mai [12] is derived from a MSCC procedure and aims for avoiding high currents at high SOCs. This is due to the fact that high current rates at elevated voltages were found to increase the likelihood of lithium plating according to the literature [9,11,12]. The approach is however expected not to be capable of preventing lithium plating under varying temperature boundary conditions. This is because the voltage ramp given in mV s^{-1} is not defined to be a function of the battery's temperature. The algorithm proposed in the work of Sieg [13] is, in contrast, expected to be capable of handling varying temperature boundary conditions, taking into consideration that the authors determined no-plating current rates for different battery temperatures using pouch-format batteries. However, the charging time observed for a fast charging procedure with temporary current limitation, for instance due to a malfunction in the charging infrastructure, is expected to be increased compared to the polarization-based approach we propose. This is due to the fact that the no-plating current introduced by Sieg [13] is determined as a function of the battery's SOC thereby depending on the distribution of lithium-ions within the solid active material, the lithium-ion distribution in the liquid phase, and on the charge transfer reaction [13]. Unforeseen limitations in current supply are however considered to cause the lithium-ion concentration along the x-coordinate within the positive and negative electrodes' solid active material composite and within the liquid electrolyte to balance. The risk for unwanted lithium plating following the temporarily occurring current limitation is accordingly reduced compared to a charging procedure without any limitation. The battery is hence capable of higher current rates for the time-period in which the critical lithium-ion concentration gradient within the electrode's solid active material particles and the liquid electrolyte is yet to be built up. The polarization-based procedure we propose is capable of providing information about the maximum current rate not causing unwanted lithium plating. This is since the full cell voltage, due to the contribution of the negative electrode's polarization, holds information about the lithium-ion distribution in the solid active material composite and the liquid electrolyte. The polarization-based procedure is furthermore considered to be capable of controlling the anode potential under varying temperature boundary conditions due to the temperature dependency of the introduced voltage threshold. The algorithms introduced by Mai [12] and Sieg [13] are implemented in our modeling framework according to the information given in the corresponding publications. However, the voltage-based procedure proposed by Mai [12] is adapted by means of an additional CV phase at 3.9 V prior to the application of the voltage ramp. The additional phase aims for better reproducing the full cell voltage profile, which is observed in an anode potential controlled simulation at the anode potential target value of 10 mV vs. Li/Li$^+$. The voltage ramp is furthermore specified to have a constant gradient of 0.25 mV s^{-1}. The procedure introduced by Sieg [13] is implemented without further adjustments. The temperature-dependent no-plating currents are thereby derived by means of simulation and stored in a 2D look-up-table as suggested by the authors [13]. Table 4 summarizes the minimum anode potentials and the inaccuracy of the regulation in each use case. The corresponding current, voltage and anode potential profiles are shown in Fig. 9.

Reference charging procedure.— It is subsequently to be evaluated whether the algorithms are capable of maintaining the anode potential target value of 10 mV vs. Li/Li$^+$ under the reference conditions (2.5C, 25 °C, and 10% SOC). The corresponding current, temperature and anode potential profiles are identified with 'Case 01' in Table 4 and Fig. 9. It is thereby shown in Fig. 9(a) and (b), that the anode potential regulation is sufficiently accurate if the polarization-based approach we propose or the current-based procedure introduced by Sieg [13] is used for current control. The minimum anode potential is found to be 9.5 mV vs. Li/Li$^+$ for the polarization-based procedure. The procedure proposed by Sieg [13] shows a similar performance with a minimum anode potential as high as 9.1 mV vs. Li/Li$^+$. However, the anode potential drops noticeable below the targeted anode potential showing a value of 5.5 mV vs. Li/Li$^+$ when the fast charging algorithm introduced by Mai [12] is applied. The RMSE is in this case calculated to be as high as 3.6 mV compared to 0.7 mV for the polarization-based approach we propose, and 1.1 mV for the algorithm introduced by Sieg [13]. The increased inaccuracy that is observed for the voltage-based procedure introduced by Mai [12] is attributed to the fact that the, not ideally linear, behavior of the full cell voltage is approximated linearly in their fast charging procedure. The polarization-based approach we propose in this study and the current-based algorithm introduced by Sieg [13] store voltage or current thresholds as a function of the charging state in a system of look-up-tables allowing for non-linear profiles. The battery

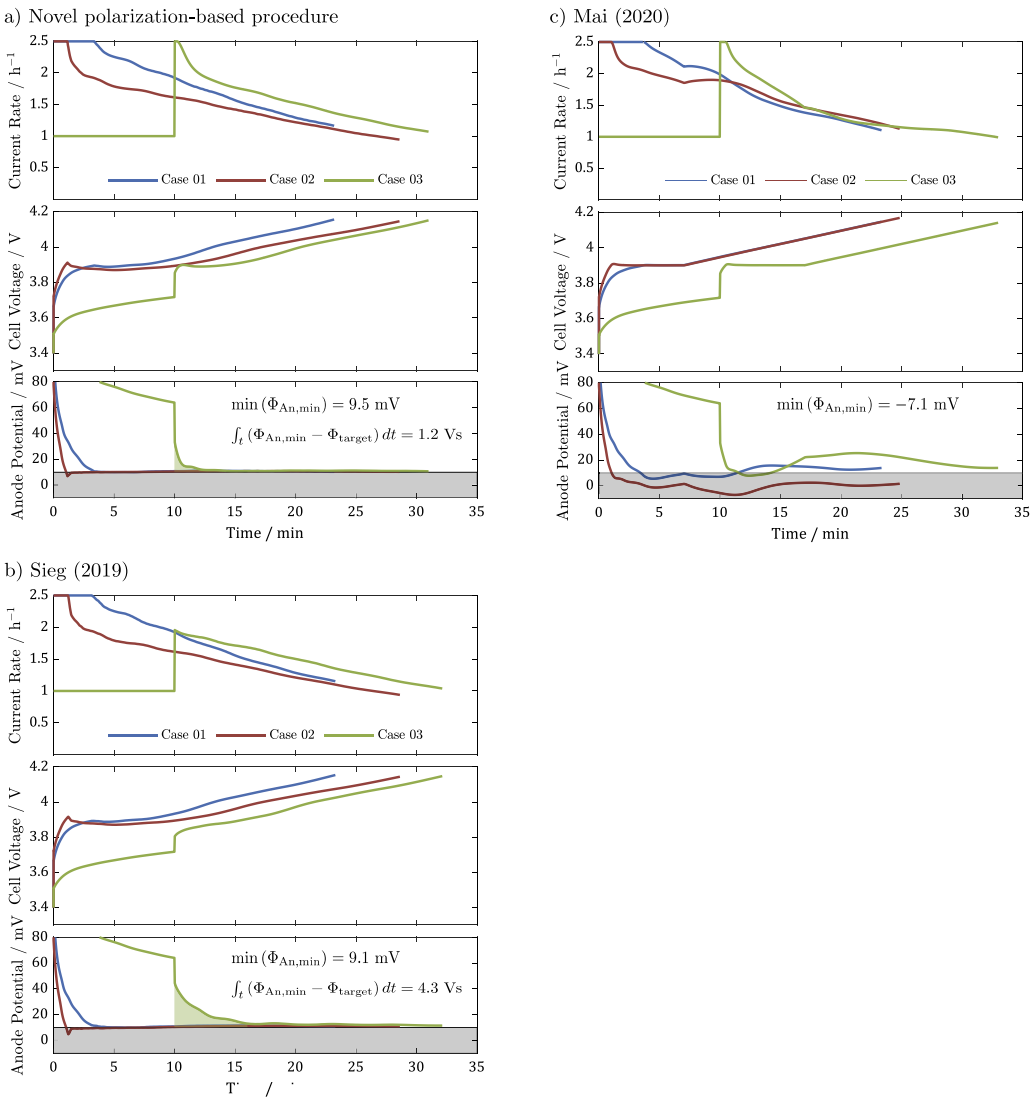

Fig. 9. Current rate, cell voltage and anode potential for polarization-based fast charge procedure (a), for the current-based fast charging protocol introduced by Sieg [13] (b) and for the voltage-based approach introduced by Mai [12] (c). The simulation case 'Case 01' represents the reference charging procedure exhibiting a maximum current rate of 2.5C, an ambient temperature of 25 °C and an initial charging state of 10% SOC. In the simulation case 'Case 02', the ambient temperature is changed to 15 °C not adapting the parameterization of the charging procedure. The simulation case 'Case 03' is similar to 'Case 01' in terms of the boundary conditions with the current rate limited to 1C for the first 10 min of the charging procedure.

Table 4
Min. anode potential and RMSE of the anode potential regulation retrieved from the simulation-based comparison of the proposed polarization-based fast charging procedure with the approaches introduced by Mai (Ref. [12]) and Sieg (Ref. [13]).

	Polarization-based		Mai (Ref. [12])		Sieg (Ref. [13])	
	$\min(\Phi_{An,min})$	RMSE	$\min(\Phi_{An,min})$	RMSE	$\min(\Phi_{An,min})$	RMSE
'Case 01'	9.9 mV	±0.7 mV	5.5 mV	±3.6 mV	9.9 mV	±1.1 mV
'Case 02'	9.5 mV	±0.6 mV	−7.1 mV	±10.7 mV	9.1 mV	±1.0 mV
'Case 03'	10.7 mV	±2.2 mV	7.9 mV	±9.7 mV	11.5 mV	±7.7 mV

behavior during fast charging is hence represented more accurately. The approach introduced by Mai [12] is consequently considered to not be capable of realizing a sufficiently accurate anode potential control, which is required to avoid hazardous lithium plating, while maintaining the minimum possible charging time. This becomes even more prominent taking into account that the charging time is found to be 23.4 min and therefore similar compared to the polarization-based procedure we propose (23.2 min) and the method introduced by Sieg [13] (23.3 min) in spite of the fact that the anode potential is found to drop below the target value of 10 mV vs. Li/Li^+ in the reference fast charging procedure.

Temperature variation.— The polarization-based fast charging procedure proposed in this study, as well as the algorithms proposed by Sieg [13] and Mai [12] are furthermore to be investigated under a temperature boundary condition that varies from the reference conditions. Thereby, the ambient temperature is reduced to 15 °C. Due to the well-known interrelation between temperature, mass and charge transport within the battery and the reaction kinetics, the reduced ambient temperature is considered to cause the risk for unwanted lithium plating to increase [9,11]. The polarization-based fast charging procedure we propose in this study, accounts for the increased plating risk utilizing a temperature-dependent threshold in the voltage-regulated phase. The

anode potential target value of 10 mV vs. Li/Li$^+$ is accordingly found to be reached in spite of the variation of the ambient temperature as shown in Fig. 9(a). Table 4 shows that the minimum anode potential and the accuracy of the anode potential regulation reach comparable values than those observed for 'Case 01'. The current-based fast charging approach introduced by Sieg [13] is similarly capable of controlling the anode potential sufficiently well, i.e. with a root-mean-square error of 0.6 mV in the case of a reduced ambient temperature. It is however to be stressed that an initial undershoot to 5 mV vs. Li/Li$^+$ is observed. A similar undershoot is to be found for the polarization-based procedure. The observed undershoot is not considered when evaluating the inaccuracy of the anode potential regulation for the aforementioned algorithms due to the fact that is caused by the non-ideally parameterized PI-controller used in our modeling framework as outlined previously. Regarding the procedure proposed by Mai [12], the anode potential is not controlled properly under varying temperature boundary conditions. This becomes prominent considering that the minimum anode potential falls below the theoretical plating onset of 0 V vs. Li/Li$^+$ when the ambient temperature is reduced to 15 °C. This behavior might however be counteracted by varying the voltage limit as well as the voltage ramp with temperature. It is furthermore considered noteworthy that the anode potential control is significantly more inaccurate compared to the other approaches when the voltage-based procedure introduced by Mai [12] is used for voltage control. The RMSE is thereby calculated to be as high as 10.7 mV for the investigated temperature reduction in 'Case 02'. This is due to the fact, that the voltage ramp is defined to be a function of time (mV s^{-1}) by the authors [12]. Therefore, the included information about the maximum full cell polarization not causing lithium plating is not linked to the battery's charging state. Hence, the procedure is not considered to allow for an anode potential control under varying temperature boundary conditions. The polarization-based procedure as well as the approach introduced by Sieg [13] are however considered to be capable of handling temperature variations.

Infrastructural current limitation.— The influence of a variations in the current boundary conditions are investigated by limiting the current rate to a maximum of 1C for the first 10 min of the charging procedure, as was outlined previously. The limitation is found to cause the battery's average temperature to decrease by approximately 7 K. This is observed independently of the charging procedure applied. The risk for unwanted lithium plating consequently increases [9,11]. However, the lithium-ion concentration along the x-coordinate within the negative electrodes active material composite is, due to the initial current limitation, expected to more balanced. The more balanced lithium-ion concentration, for its part, reduces the risk of unwanted lithium plating [13]. As a result, the prediction of the lithium plating risk complicates, which makes regulating the current at the battery's physical limits a difficult task. The polarization-based fast charging procedure we propose is nevertheless capable of controlling the anode potential accurately as shown in Fig. 9(a). The anode potential almost immediately reaches the target value of 10 mV vs. Li/Li$^+$ after the limitation in the available charging current has been overcome. The deviation of the anode potential from its target value was calculated to be as low as 1.2 Vs for the polarization-based procedure. The voltage-based procedure introduced by Mai [12] is however found not to be capable of controlling the anode potential in the event of an initial current limitation. The inaccuracy of the anode potential control is thereby increased by 6.1 mV from 3.6 mV to 9.7 mV. This is again to be explained by the missing link between the specified voltage ramp and the battery's charging state. The current-based procedure introduced by Sieg [13] is similarly not capable of adapting to the variation in the current boundary condition. This is due to the fact that the algorithm does not allow for the realization of a feedback-control since the changed full cell polarization, following the limitation in the available charging current, is not captured in the current-based approach. The inaccuracy following the current limitation, indicated by the highlighted area in Fig. 9, is found to be as high as 4.3 Vs. The RMSE of the anode potential with respect to its target value of 10 mV vs. Li/Li$^+$ is calculated to be as high as 7.7 mV for the entire charging procedure. This is significantly higher compared to the polarization-based procedure we propose, which shows a value of 2.2 mV for the respective use case. However, the anode potential is not found to drop below the target value. The hazardous lithium plating phenomena is therefore not provoked. Instead, the current limitation causes the charging time to increase by 2 min compared to the polarization-based approach if the algorithm introduced by Sieg [13] is used for current control. The increase in charging time is expected to be more pronounced if the current limitation occurs at higher SOCs. This is due to the fact that the no-plating current consistently decreases with increasing SOC in the respective algorithm [13].

4. Conclusion

In this work, a novel fast charging procedure is proposed that uses a polarization-induced correlation between cell voltage and anode potential for current control. A correlation analysis is performed, that reveals an approximately linear interrelation between cell voltage and anode potential. The relation is only marginally affected by variations in the operational parameters (current, temperature and the initial SOC). Nevertheless, an impact on the accuracy of the anode potential regulation is observed. The polarization-based procedure is accordingly expected to show best accuracies for current rates up to 2.5C and temperatures below 20 °C. This is due to the fact that the battery's internal resistance, is according to the work of Jow [38], dominated by the negative electrode under these respective conditions. The influence of time-dependent processes on the relation between cell voltage and anode potential is investigated by means of a two-step CC profile. It is thereby observed, that the contributions of the positive and negative electrode to the full cell polarization vary if different initial current rates and various current differences are applied, or if the SOC of the switching point in the current profile is changed. An impact on the accuracy, with which the anode potential is predicted using the relation, is found. However, the most prominent changes in the polarization are found to decay within 180 s suggesting that the correlation is suitable for predicting the gradient of the anode potential under the assumption of a steady-state battery state. This is considered a distinctive constraint for the usability of the relation in fast charging procedures. The correlation is nevertheless utilized for the purpose of deriving a voltage threshold correlating with an anode potential target value of 10 mV vs. Li/Li$^+$. The voltage threshold is used in the proposed fast charging procedure as reference curve for a voltage-regulated phase. It is found, in a simulation study that the voltage threshold is, similar to the relation between cell voltage and anode potential, affected by the operational parameters. Most pronounced influences are observed for variations in temperature and the initial SOC. However, this is not considered a constraint for the practicability of the voltage threshold in the proposed fast charging procedure as long as the influences of temperature and the initial SOC are taken into consideration properly in the fast charging algorithm. The implementation of the anode potential regulation by means of the introduced voltage threshold is considered a significant advantage most notably for usage in embedded systems. This is due to the fact that the computationally extensive Newman-type P2D model is only to be used offline in order to derive the correlation information and for the controller-parameterization, resulting in significantly reduced hardware requirements. The introduced approach is subsequently compared to recently proposed fast charging procedures [12,13] in terms of the performance of the implemented anode potential control under varying current and temperature boundary conditions. The proposed procedure thereby shows the highest accuracy in terms of the anode potential control as well as an advantage in charging time in the case of a temporary limitation in the available charging current, due to

Table A.1
P2D model parameterization set for the investigated NMC-graphite battery. Parameters were adopted from the work of Hamar [16].

Geometry	Symbol	Unit	Graphite (C)	Separator	Nickel-rich (NMC-811)
Thickness[a]	t	m	8.50e−05	2.50e−05	5.50e−05
Density	ρ	g cm^{-3}	2.24		4.06
Particle radius[b]	r_P	m	1.00e−05		8.80e−06
Active material fraction[b]	ϵ_s	–	0.68		0.68
Inactive fraction[b]	$\epsilon_{s,na}$	–	0.03		0.03
Porosity	ϵ_l	–	0.29	0.40	0.29
Bruggeman coefficient[e]	α_B	–	2.50	2.50	1.80
Thermodynamics					
Equilibrium potential[c]	E_{eq}	V vs. Li/Li$^+$	Ref. [29]		[29]
Entropic coefficient[c]	$\frac{\partial E_{eq}}{\partial T}$	V K^{-1}	Ref. [29]		[29]
Stoichiometry at 100% SOC[a]	$\theta_{100\%}$	–	0.8652		0.2180
Stoichiometry at 0% SOC[a]	$\theta_{0\%}$	–	0.0100		0.9587
Gravimetric loading	b_g	mAh g^{-1}	347.85		223.2
Maximum Concentration[b]	$c_{s,max}$	mol m^{-3}	28,548		50,060
Transport					
Solid diffusivity[b,d]	D_s	m^2 s^{-1}	1.60e−14		6.00e−14
Specific activation[b,d]	$\frac{E_{a,D_s}}{R}$	K	1,200		1,200
Solid conductivity	σ_s	S m^{-1}	1,000		20.00
Film resistance	Rf	Ω m^2	3.30e−04		1.30e−04
Kinetics					
Reaction rate constant[b,d]	k	m s^{-1}	6.40e−09		1.68e−09
Specific activation[b,d]	$\frac{E_{a,k}}{R}$	K	3,600		3,600
Transfer coefficient	$\alpha_{a/c}$	–	0.50		0.50
Ref. concentration	$c_{l,ref}$	mol m^{-3}	1,200		1,200

[a]Measured.
[b]Estimated.
[c]Literature.
[d]Arrhenius law (Ref. [39]): $k = \left(\frac{^*E_{a,i}}{R}\frac{(T-298\ [K])}{T\cdot 298\ [K]}\right)$.
[e]Effective transport correction according to Bruggeman (Ref. [40]).

Table A.2
0D thermal model parameterization set for the investigated NMC/graphite battery. Parameters were adopted from the work of Hamar [16].

	Symbol	Unit	NMC/graphite
Density	ρ	kg m^{-3}	2354.42
Volume	V	m^3	4.20e−04
Heat transfer coefficient	h	W kg^{-1} K^{-1}	6.00
Specific heat capacity	c_p	J kg^{-1} K^{-1}	880.00
Surface area	A	m^2	7.60e−02

infrastructural limitations. It is conclusively to be stressed that the experimental validation of the electrochemical-thermal model, that is used in this work, as well as the validation of the proposed polarization-based fast charging procedure is, though considered important, out of scope of this work. The simulation-based analysis of the accuracy of the implemented anode potential regulation under varying current and temperature boundary conditions, and the investigation of the influence of electrode-heterogeneities is however considered crucial for the use of a polarization-based fast charging approach in technology relevant applications.

CRediT authorship contribution statement

C. Zoerr: Conceptualization, Methodology, Formal analysis, Writing – original draft, Visualization. **J.J. Sturm:** Conceptualization, Methodology, Writing – original draft. **S. Solchenbach:** Conceptualization, Methodology, Writing – review & editing. **S.V. Erhard:** Conceptualization, Supervision, Writing – review & editing. **A. Latz:** Supervision, Writing – review & editing.

Declaration of competing interest

The authors declare the following financial interests/personal relationships which may be considered as potential competing interests: Christoph Zoerr reports financial support was provided by Bayerische Motoren Werke AG. Christoph Zoerr, Johannes Sturm, Sophie Solchenbach and Simon Erhard report a relationship with Bayerische Motoren Werke AG that includes: employment and funding grants. Christoph Zoerr and Simon Erhard have patent # DE 10 2021 108 085 A1 issued to Bayerische Motoren Werke AG.

Data availability

The authors do not have permission to share data.

Acknowledgments

This work was funded by the BMW Group and was performed in cooperation with Helmholtz Institute Ulm for Electrochemical Energy Storage.

Appendix A. P2D model parameterization

See Tables A.1 and A.2.

Appendix B. Controller setup

The voltage controlled current regulation in the second phase of the proposed polarization-based fast charging procedure is implemented by means of a simple PI-controller. The general controller equation is given by the expression

$$y(t) = k_p e(t) + k_i \int_0^t e(t)\,dt \tag{B.1}$$

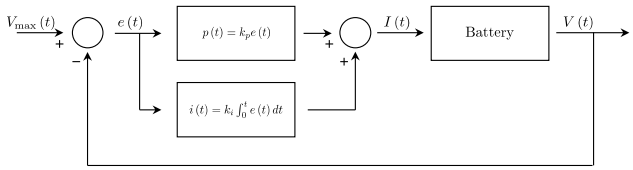

Fig. B.1. Schematic setup of the PI controller used for the voltage-regulated phase in the proposed polarization-based fast charging procedure. The difference between the threshold $V_{\max}(t)$ and the full cell voltage $V_{\text{cell}}(t)$ is given gy $e(t)$. The controller parameters k_p and k_i are used to calculate the charging current $I(t)$ the battery is subjected to.

where k_p and k_i are the parameters of the controller and $e(t)$ is the controller offset that is in this work considered to be the difference between the full cell voltage and the voltage threshold. The controller output $y(t)$ represents the charging current the battery is subjected to. It depends on the controller offset, on the parameters of the PI-controller as well as (due to the integrative part) on the respective time t an offset is detected. The controller parameters for a sufficiently accurate regulation are expected to be affected by the battery chemistry and the respective boundary conditions (e.g. current, temperature and SOC). The controller setup is illustrated in Fig. B.1.

Appendix C. Supplementary data

Supplementary material related to this article can be found online at https://doi.org/10.1016/j.est.2023.108234.

References

[1] A. Tomaszewska, Z. Chu, X. Feng, S. O'Kane, X. Liu, J. Chen, C. Ji, E. Endler, R. Li, L. Liu, Y. Li, S. Zheng, S. Vetterlein, M. Gao, J. Du, M. Parkes, M. Ouyang, M. Marinescu, G. Offer, B. Wu, Lithium-ion battery fast charging: A review, ETransportation 1 (15) (2019) 100011.

[2] Y. Gao, X. Zhang, Q. Cheng, B. Guo, J. Yang, Classification and review of the charging strategies for commercial lithium-ion batteries, IEEE Access 7 (2019) 43511–43524.

[3] Y. Gao, J. Jiang, C. Zhang, W. Zhang, Z. Ma, Y. Jiang, Lithium-ion battery aging mechanisms and life model under different charging stresses, J. Power Sources 356 (2017) 103–114.

[4] D. Anseán, M. Dubarry, A. Devie, B.Y. Liaw, V.M. García, J.C. Viera, M. González, Fast charging technique for high power LiFePO4 batteries: A mechanistic analysis of aging, J. Power Sources 321 (2016) 201–209.

[5] C. Chen, F. Shang, M. Salameh, M. Krishnamurthy, Challenges and advancements in fast charging solutions for EVs: A technological review, in: 2018 IEEE Transportation Electrification Conference and Expo (ITEC), IEEE, 2018, pp. 695–701, 13.06.2018 - 15.06.2018.

[6] M. Hao, J. Li, S. Park, S. Moura, C. Dames, Efficient thermal management of Li-ion batteries with a passive interfacial thermal regulator based on a shape memory alloy, Nat. Energy 3 (10) (2018) 899–906.

[7] S.S. Zhang, The effect of the charging protocol on the cycle life of a Li-ion battery, J. Power Sources 161 (2) (2006) 1385–1391.

[8] N. Legrand, B. Knosp, P. Desprez, F. Lapicque, S. Raël, Physical characterization of the charging process of a Li-ion battery and prediction of Li plating by electrochemical modelling, J. Power Sources 245 (2014) 208–216.

[9] T. Waldmann, M. Kasper, M. Wohlfahrt-Mehrens, Optimization of charging strategy by prevention of lithium deposition on anodes in high-energy lithium-ion batteries – electrochemical experiments, Electrochim. Acta 178 (2015) 525–532.

[10] T. Waldmann, B.-I. Hogg, M. Wohlfahrt-Mehrens, Li plating as unwanted side reaction in commercial Li-ion cells – A review, J. Power Sources 384 (2018) 107–124.

[11] T. Waldmann, B.-I. Hogg, M. Kasper, S. Grolleau, C.G. Couceiro, K. Trad, B.P. Matadi, M. Wohlfahrt-Mehrens, Interplay of operational parameters on lithium deposition in lithium-ion cells: Systematic measurements with reconstructed 3-electrode pouch full cells, J. Electrochem. Soc. 163 (7) (2016) A1232–A1238.

[12] W. Mai, A.M. Colclasure, K. Smith, Model-instructed design of novel charging protocols for the extreme fast charging of lithium-ion batteries without lithium plating, J. Electrochem. Soc. 167 (8) (2020) 080517.

[13] J. Sieg, J. Bandlow, T. Mitsch, D. Dragicevic, T. Materna, B. Spier, H. Witzenhausen, M. Ecker, D.U. Sauer, Fast charging of an electric vehicle lithium-ion battery at the limit of the lithium deposition process, J. Power Sources 427 (2) (2019) 260–270.

[14] S. Tippmann, D. Walper, L. Balboa, B. Spier, W.G. Bessler, Low-temperature charging of lithium-ion cells part I: Electrochemical modeling and experimental investigation of degradation behavior, J. Power Sources 252 (4) (2014) 305–316.

[15] M. Abdel-Monem, K. Trad, N. Omar, O. Hegazy, P. van den Bossche, J. van Mierlo, Influence analysis of static and dynamic fast-charging current profiles on ageing performance of commercial lithium-ion batteries, Energy 120 (2017) 179–191.

[16] J.C. Hamar, S.V. Erhard, C. Zoerr, A. Jossen, Anode potential estimation in lithium-ion batteries using data-driven models for online applications, J. Electrochem. Soc. 168 (3) (2021) 030535.

[17] X. Lin, Real-time prediction of anode potential in li-ion batteries using long short-term neural networks for lithium plating prevention, J. Electrochem. Soc. 166 (10) (2019) A1893–A1904.

[18] J. Remmlinger, S. Tippmann, M. Buchholz, K. Dietmayer, Low-temperature charging of lithium-ion cells Part II: Model reduction and application, J. Power Sources 254 (1) (2014) 268–276.

[19] J. Sturm, S. Ludwig, J. Zwirner, C. Ramirez-Garcia, B. Heinrich, M.F. Horsche, A. Jossen, Suitability of physicochemical models for embedded systems regarding a nickel-rich, silicon-graphite lithium-ion battery, J. Power Sources 436 (12) (2019) 226834.

[20] A. Jokar, B. Rajabloo, M. Désilets, M. Lacroix, Review of simplified Pseudo-two-Dimensional models of lithium-ion batteries, J. Power Sources 327 (6058) (2016) 44–55.

[21] A. Seaman, T.-S. Dao, J. McPhee, A survey of mathematics-based equivalent-circuit and electrochemical battery models for hybrid and electric vehicle simulation, J. Power Sources 256 (12) (2014) 410–423.

[22] P.W.C. Northrop, B. Suthar, V. Ramadesigan, S. Santhanagopalan, R.D. Braatz, V.R. Subramanian, Efficient simulation and reformulation of lithium-ion battery models for enabling electric transportation, J. Electrochem. Soc. 161 (8) (2014) E3149–E3157.

[23] A.M. Bizeray, S. Zhao, S.R. Duncan, D.A. Howey, Lithium-ion battery thermal-electrochemical model-based state estimation using orthogonal collocation and a modified extended Kalman filter, J. Power Sources 296 (6) (2015) 400–412.

[24] Q.Q. Liu, R. Petibon, C.Y. Du, J.R. Dahn, Effects of electrolyte additives and solvents on unwanted lithium plating in lithium-ion cells, J. Electrochem. Soc. 164 (6) (2017) A1173–A1183.

[25] M. Doyle, T.F. Fuller, J. Newman, Modeling of galvanostatic charge and discharge of the lithium/polymer/insertion cell, J. Electrochem. Soc. 140 (6) (1993) 1526–1533.

[26] T.F. Fuller, M. Doyle, J. Newman, Relaxation phenomena in lithium–Ion–Insertion cells, J. Electrochem. Soc. 141 (4) (1994) 982–990.

[27] T.F. Fuller, M. Doyle, J. Newman, Simulation and optimization of the dual lithium ion insertion cell, J. Electrochem. Soc. 141 (1) (1994) 1–10.

[28] S.V. Erhard, P.J. Osswald, J. Wilhelm, A. Rheinfeld, S. Kosch, A. Jossen, Simulation and measurement of local potentials of modified commercial cylindrical cells, J. Electrochem. Soc. 162 (14) (2015) A2707–A2719.

[29] J. Sturm, A. Rheinfeld, I. Zilberman, F.B. Spingler, S. Kosch, F. Frie, A. Jossen, Modeling and simulation of inhomogeneities in a 18650 nickel-rich, silicon-graphite lithium-ion cell during fast charging, J. Power Sources 412 (13) (2019) 204–223.

[30] S. Hein, A. Latz, Influence of local lithium metal deposition in 3D microstructures on local and global behavior of Lithium-ion batteries, Electrochim. Acta 201 (2016) 354–365.

[31] D. Bernardi, E. Pawlikowski, J. Newman, A general energy balance for battery systems, J. Electrochem. Soc. 132 (1) (1985) 5–12.

[32] A. Nyman, T.G. Zavalis, R. Elger, M. Behm, G. Lindbergh, Analysis of the polarization in a Li-Ion battery cell by numerical simulations, J. Electrochem. Soc. 157 (11) (2010) A1236.

[33] A. Jossen, Fundamentals of battery dynamics, J. Power Sources 154 (2) (2006) 530–538.

[34] S.V. Erhard, P.J. Osswald, P. Keil, E. Höffer, M. Haug, A. Noel, J. Wilhelm, B. Rieger, K. Schmidt, S. Kosch, F.M. Kindermann, F. Spingler, H. Kloust, T. Thoennessen, A. Rheinfeld, A. Jossen, Simulation and measurement of the current density distribution in lithium-ion batteries by a multi-tab cell approach, J. Electrochem. Soc. 164 (1) (2017) A6324–A6333.

[35] J. Sturm, A. Frank, A. Rheinfeld, S.V. Erhard, A. Jossen, Impact of electrode and cell design on fast charging capabilities of cylindrical lithium-ion batteries, J. Electrochem. Soc. 167 (13) (2020) 130505.

[36] Y. Ji, Y. Zhang, C.-Y. Wang, Li-ion cell operation at low temperatures, J. Electrochem. Soc. 160 (4) (2013) A636–A649.

[37] C. Qiu, G. He, W. Shi, M. Zou, C. Liu, The polarization characteristics of lithium-ion batteries under cyclic charge and discharge, J. Solid State Electrochem. 23 (6) (2019) 1887–1902.

[38] T.R. Jow, S.A. Delp, J.L. Allen, J.-P. Jones, M.C. Smart, Factors limiting Li + charge transfer kinetics in Li-ion batteries, J. Electrochem. Soc. 165 (2) (2018) A361–A367.

[39] S. Arrhenius, Über die reaktionsgeschwindigkeit bei der inversion von rohrzucker durch säuren, Z. Phys. Chem. 4 (1) (1889).

[40] D.A.G. Bruggeman, Berechnung verschiedener physikalischer Konstanten von heterogenen Substanzen. I. Dielektrizitätskonstanten und Leitfähigkeiten der Mischkörper aus isotropen Substanzen, Ann. Phys. 416 (7) (1935) 636–664.